Received 20 November 2023; revised 18 December 2023; accepted 25 December 2023. Date of publication 2 January 2024; date of current version 26 March 2024.

Digital Object Identifier 10.1109/OJAP.2023.3349358

4×4 UWB Phased Array Antenna With >51° Far-Field Scanning Range for Wireless Power Transfer Application

ADNAN BASIR PATWARY (Member, IEEE) AND IFANA MAHBUB (Senior Member, IEEE)

Department of Electrical and Computer Engineering, The University of Texas at Dallas, Richardson, TX 75080, USA

CORRESPONDING AUTHOR: A. B. PATWARY (e-mail: adnanbasir.patwary@utdallas.edu)

This work was supported by the Defense Advanced Research Projects Agency (DARPA) under Grant W911NF-23-1-0029.

ABSTRACT Wireless power transfer (WPT) using far-field microwave radiation beam can be used to power unmanned aerial vehicles (UAVs) thus eliminating the need to land on the ground to charge. In a distributed WPT system, impulse radio ultrawideband (IR-UWB) signals can provide continuous power at the receiver end with a high rectification efficiency. Such far-field based distributed WPT systems require high gain ultrawideband (UWB) antenna arrays with a unidirectional radiation patterns and beam steering capability. This paper proposes a 4×4 phased array antenna with an ultrawideband (UWB) operating frequency range of $7.5 - 8.5$ *GHz* and 20.9 *dBi* gain. The novelty of this work lies in the design of a single unit antenna to achieve UWB operation while maintaining high gain and unidirectional radiation pattern. Another contribution of this work is the determination of the array element spacing based on the theoretical modeling and simulation and measurement based validation to achieve the highest gain, minimum coupling coefficient, and lower side lobe level (SLL). In order to achieve beam steering, each 2×2 subarray is considered as a single quadrant thus dividing the 4×4 phased array antenna into four quadrants where all 16 single elements are individually fed. The far-field radiation beam is steered by controlling the phase difference between each quadrant. The proposed phased array antenna achieves a scanning range $> 51°$ with 28° half power beam width (HPBW), gain ranging from 15.4 *dBi* to 20.9 *dBi*, and a maximum scanning loss of 2.8 *dB* over the UWB operating frequency range.

INDEX TERMS Wireless power transfer, microstrip antenna, ultrawideband antenna, phased array antenna, UWB phased array antenna, far-field beamsteering.

I. INTRODUCTION

WIRELESS power transfer (WPT) is an emerging technology that is being extensively researched in recent times. WPT can help to maintain continuous power delivery to electronic devices by decreasing the use of cables and batteries which act as a constraint in the power supply as well as hinder mobility. The technique of WPT using microwave far-field radiation beam has been developed mainly with the priority to be used in the aerospace field, enabling wireless power transfer from the ground station to an unmanned aircraft flying through the stratosphere [1], [2]. Onboard batteries are conventionally used to power unmanned areal vehicles (UAVs) which increases the payloads on the UAVs and increases the power requirement thus reducing the flight time. WPT can be an effective solution to this problem as it reduces the need for bulky batteries and the need to land to recharge thus providing a continuous flight. Fig. 1 depicts a distributed WPT system for UAVs where the UAVs can be charged from the base station along with nearby UAVs when the onboard battery runs low. There are two prevailing approaches of implementing WPT: (a) non-radiative coupling in the near-field, and (b) far-field radiation based power beaming. Near-field WPT uses inductive and inductive/magnetic resonance coupling between the transmitter (TX) and the receiver (RX) which provides a short range (< 20 *cm*) WPT [3], [4], [5]. In near-filed coupling based WPT, the electromagnetic fields limit the wave propagation to a minimal amount because of the

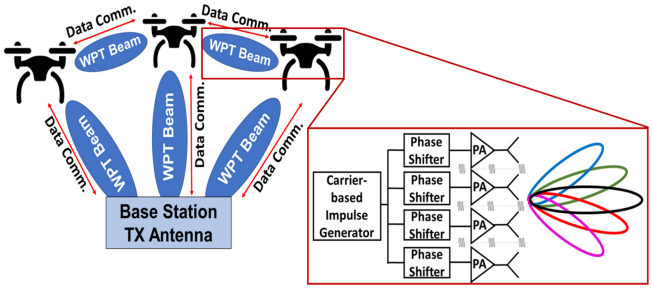

FIGURE 1. Far-field based WPT system.

power attenuation at the rate of $1/d^3$, where d represents the distance between the TX and the RX antennas [6].

Far-field radiation is a more practical alternative for WPT over a longer distance. Directive beamforming is a method in far-field RF technology where the signal is transmitted through antennas with narrow beam radiation and high gain [7]. The major obstacle of far-field based WPT is the free space path loss which can be reduced through directive beamforming and achieving a pencil beam. A directive beamforming based WPT is proposed in [8] which provides wireless power over 1 m distance with 3.1% power transfer efficiency (PTE) by using 5.8 GHz continuous signal and 15 dBi gain antenna. To enhance the overall efficiency of a distributed WPT system, impulse based radio signal can be used. Carrier based impulse radio ultrawideband (IR-UWB) system can achieve high peak-to-average power ratio (PAPR) and provide high controllability and selectivity by applying phase-shifting in the input signal to control the far-field radiation beam direction [9], [10]. The high PAPR of the IR-UWB provides efficient rectification at the receiver compared to the same power transmitted over continuous waves at a certain time [11]. The impulse synchronization of IR-UWB can provide constant power at the receiver of a distributed system and reduces the loss due to the phase incoherence of the received signal. However, an ultrawideband antenna with a high gain is required in order to implement an IR-UWB based WPT system as the energy of an IR-UWB is spread over a wide frequency spectrum. Also, in order to wirelessly power mobile devices such as UAVs, the far-field beam needs to be steered instantaneously. The antennas that are used to power the UAV can be mechanically steered but that requires additional power and control systems to mechanically rotate the antennas. Electrical steering can be implemented to steer the far-field beam and with the combination of mechanical steering a wide range can be achieved. Fig. 1 depicts the far-field-based WPT system for a distributed system where the UAV can receive wireless power from the base station to power themselves along with relaying the power wirelessly to a nearby UAV. The receiver antenna of a UAV in such system is required to be omnidirectional to receive the multiple wireless power beams from different directions. The WPT transmitter antenna in the UAV is required to be unidirectional to focus the wireless power and the far-field beam must be steerable. This paper focuses on the WPT transmitter antenna on a UAV. Based on the discussion mentioned above the drone-to-drone IR-UWB far-field WPT system for UAVs in a distributed system with 5 m distance would require transmitter antennas with a high gain (> 15 dBi), ultra-wide bandwidth (> 500 MHz), unidirectional radiation pattern, and radiation beam scanning range of $> 50°$. Conventional small UAVs have fuselage $< 100 \times 40$ cm^2 which restricts the antenna size [12]. Fig. 1 also depicts the far-field based WPT system for UAVs where the far-field beam can be steered by implementing phase shift in the signals.

Conventional antennas used for WPT are traditionally narrowband antennas. A 5.8 GHz phased array antenna is designed in [13] which has 21 dBi gain and a unidirectional radiation beam where the far-field beam can be maneuvered using microprocessor controlled phase delay in input signal at the array elements. However, the proposed antenna in [13] operates at a narrowband which is not suitable for IR-UWB based WPT systems. Another 5.8 GHz omnidirectional antenna used for WPT is proposed in [14] which has 980 MHz bandwidth and is suitable for UWB application but it has a low gain (7 dBi). A phased array antenna with 4×4 element structure has been designed in [15] where far-field radiation beam direction is changed by exciting different antennas in the phased array which achieves inconsistent gain over the scanning range. The antenna proposed in [15] also has a narrowband (100 MHz) at the center frequency of 5.8 GHz which is not suitable for the pulse based WPT. A 5.8 GHz phased array system is proposed in [16] where the far-field beam is controlled by power-variable phased controlled magnetrons which achieved 24.9 dBi gain but the scanning range achieved was only $\pm 3°$.

A 4×4 phased array antenna has been proposed in this work which achieves an UWB operating frequency, high gain, and a unidirectional far-field radiation beam that can be steered with the change in the input signal's phases at each 2×2 sub-array quadrants. The single element of the phased array is designed to have a UWB operating frequency with a unidirectional radiation pattern and a high gain. A theoretical and simulation based analysis is done to determine the optimum array element spacing to attain the achievable gain. Each 2×2 subarray of the proposed antenna has been considered a quadrant dividing the whole antenna into four quadrants. All individual antennas in the 2×2 subarray quadrant are fed with the same signal. The quadrature based feeding system is used as it reduces the active component needed to excite the antenna by $1/4^{th}$ and is advantageous when the system is needed to be scaled up. By providing changes in the input phase difference at each quadrant, the far-field beam direction is maneuvered.

The novelty of this work lies in the design and modeling of the single unit antenna, analysis to achieve optimum array spacing to achieve high gain, and quadrature based feeding along with phase combination analysis to achieve constant scanning range over the operating frequency. This

work has the following contributions which yield the novelty of this work: (1) Design of a novel single unit antenna to create the 4×4 array. The single unit antenna is designed in four steps that implements the inclusion of strategically placed slots to alter the current distribution in the antenna and achieve a UWB operating frequency ($7.5 - 8.5$ *GHz*) whilst achieving a unidirectional radiation pattern and a high gain (7.4 *dBi*). The design steps are described in detail to explain the necessity of the addition of the slots based on the current distribution. The antenna is designed to maintain the size restrictions to be placed in a small UAV while achieving better performance than the conventional wideband unit antennas. (2) Theoretical calculation and EM simulation-based analysis to determine the optimum array spacing value of the proposed UWB phased array antenna with single unit antenna dimension $> 0.6\lambda$. An EM simulation-based analysis is performed for the 2×2 array for varying array spacing to determine the optimum array spacing value at which the side lobe level (SLL) is low (< -15 *dB*) and the coupling is minimum (< -28 *dB*) whilst maintaining a high gain. The EM simulation-based optimized array spacing is further validated by calculating the array factor (AF) and the gain of the 4×4 array at varying array spacing. (3) Implementation of a 2×2 array quadrant based far-field beam steering method. In this method the far-field beam of the 4×4 array is controlled by providing phase difference at each 2×2 array quadrant. A simulation based analysis was done to determine the input phase differences which is also experimentally validated. (4) Design and fabrication of 1×4 power divider/combiner to perfectly align with the antenna feed of each 2×2 sub-array quadrant thus reducing the losses due to the cables. The combiner is designed to have low insertion loss (< 0.65 *dB*) and UWB operation while covering the bandwidth (BW) of the antenna and provide a similar phased signal at each element of the 2×2 sub-array quadrants. (5) Development and performance analysis of the compact beam steering antenna system with the proposed antenna, combiner, and beam steering method. The system achieves a wide beam scanning with a high gain. The implementation of the 2×2 array quadrant based feeding and beam steering reduces the number of active elements by $1/4^{th}$. The organization of the paper is as follows: Section II discusses the antenna design and modeling and the $1 : 4$ combiner design to feed each quadrant; Section III discusses the simulated and measured results, the beam steering, and WPT measurements; followed by concluding remarks presented in Section IV.

II. DESIGN AND MODELING

The design and simulated performance of a 4×4 phased array antenna with preliminary simulation results has been briefly discussed in our previous work [17]. The antenna designed in our previous work has been modified by optimizing the spacing between the array elements and the measured performance of the modified antenna is presented in this paper. The 4×4 phased array antenna is modeled on a

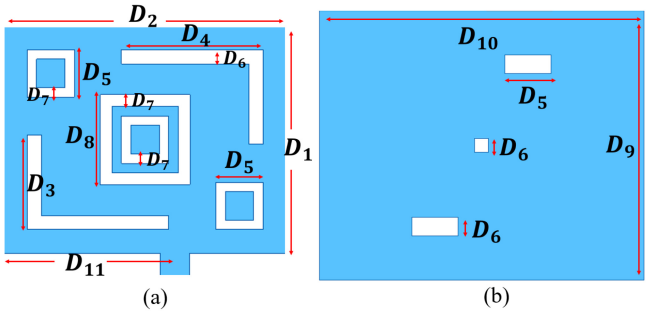

FIGURE 2. Single unit antenna (a) Front (radiating patch) and (b) bottom (ground patch) where $D_1 = 22$, $D_2 = 27.5$, $D_3 = 10$, $D_4 = 15$, $D_5 = 5$, $D_6 = 1.5$, $D_7 = 1$, $D_8 = 11.5$, $D_9 = 27$, $D_{10} = 32.5$, and $D_{11} = 17$ (unit: mm).

1.53 *mm* thick FR4 substrate with $\epsilon_r = 4.4$, and tangent loss, $tan_d = 0.02$. For the conductive ground and radiating metal patch, copper (Cu) with 0.035 *mm* thickness has been chosen. High Frequency Structure Simulator (HFSS) design module by ANSYS Electronic Desktop and Advanced Design System (ADS) by Keysight were used to model and simulate the antenna.

A. SINGLE UNIT ANTENNA DESIGN

The proposed 4×4 phased array antenna consists of 16 single unit patch antennas. The single unit antenna is designed to operate in the UWB frequency band ($3.1 - 10.6$ *GHz*), possess ultrawide bandwidth (> 500 *MHz*), high gain (> 5 *dBi*), unidirectional radiation pattern, and low side lobe level (SLL). The dimension of the single unit antenna is restricted to 25 *mm* so that when the array is created with proper spacing, it does not surpass the dimensions of the UAVs fuselage. To design a UWB phased array, conventionally wideband antennas such as bow-tie, ME dipole, and U-slot microstrip antennas are used as the unit antenna. Although bow-tie dipole antennas achieve wide bandwidth they have relatively lower gain, bidirectional radiation pattern, and are larger in size [18], [19], [20]. Magnetoelectric (ME) dipole antennas can achieve wide bandwidth, high gain, and unidirectional radiation patterns but they are larger in size and have complex designs [21], [22], [23] making them unsuitable for UAV implementation. *U*-slot microstrip antennas have a simpler design as they are designed by creating a *U*-shaped slot in the microstrip patch which enables it to achieve a wide bandwidth and high gain within the UWB frequency range [24], [25], [26]. However the *U*-slot antennas do not achieve a unidirectional radiation pattern and are conventionally larger in size. A novel modified slotted patch antenna is proposed as the single unit antenna in this paper. The antenna is designed in steps to achieve the desired operating frequency, bandwidth, gain, and radiation pattern while maintaining the above-mentioned size restriction.

The design architecture of the single element antenna along with the design parameters are shown in Fig. 2. The design process of the single unit antenna is divided into

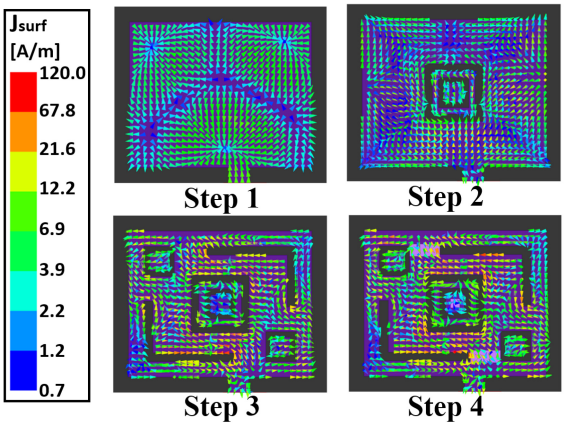

FIGURE 3. Single unit antenna design steps and current distribution at each design step for 8.4 *GHz*.

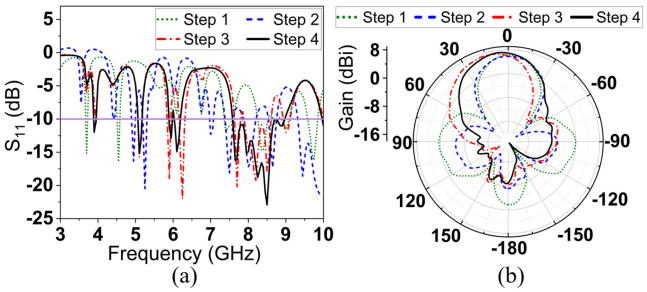

FIGURE 4. (a) S-parameter and (b) Radiation Pattern change at 8.4 *GHz* for each design step of single unit antenna.

four steps. The step-by-step design process of the single unit antenna is depicted in Fig. 3 which also includes the current distribution throughout the antenna in each design step. Fig. 4(a) and (b) show the changes in S_{11} and radiation pattern respectively of the single unit antenna at each design step. The single unit antenna is a 27.5×22 mm^2 antenna where the design is based on a basic rectangular patch antenna resonating at 3.3 *GHz* which is at the lower range of the UWB frequency band. Afterward the single element is then further modified to achieve an ultrawide bandwidth at the upper bands of the UWB frequency range.

In the first step a rectangular patch antenna of $D_2 \times D_1$ is designed where the dimensions of the D_1 and D_2 are determined using equations (1), (2), and (3) in order to achieve an operating frequency of 3.3 *GHz* [27]. In equations (1), (2), and (3), f_0 is the desired operating frequency (3.3 *GHz*), ϵ_r is the dielectric constant of the substrate (4.4), ϵ_{eff} is the effective dielectric constant, and h is the dielectric substrate's height (1.57 *mm*).

$$D_2 = \frac{c}{2f_0\sqrt{\left(\frac{1+\epsilon_r}{2}\right)}} \tag{1}$$

$$\epsilon_{eff} = \frac{1+\epsilon_r}{2} + \frac{\epsilon_r - 1}{2}\frac{1}{\sqrt{\left(1+\frac{12h}{D2}\right)}} \tag{2}$$

$$D_1 = \frac{c}{f_0\sqrt{e_{eff}}} - 0.824\left(\frac{(e_{eff}+0.3)(D2/h+0.264)}{(e_{eff}-0.258)(D2/h+0.8)}\right) \tag{3}$$

The antenna is fed using a 50 Ω microstrip feed line. A simulation based analysis was performed using Keysight ADS to estimate the feed line connection point in the antenna where the input impedance is approximately 50 Ω. The position in the antenna where the feed line is connected and where the impedance is around 50 Ω is located 3.5 *mm* to the right from the center point of the antenna As shown in Fig. 2. After step 1 the antenna achieves a resonance at 3.25 *GHz* which can be observed from Fig. 4(a). It also shows that the antenna achieves a higher order resonance at 4.75 *GHz*, 7.5 *GHz*, 8.4 *GHz*, and 9.8 *GHz* within the UWB frequency band. The antenna achieves a gain of 5.3 *dBi* and an omnidirectional radiation pattern with multiple side lobes which can be observed in Fig. 4(b). The rectangular patch antenna designed in step 1 has two higher order resonant frequencies at 7.5 *GHz* and 8.4 *GHz* which are within close range and the subsequent design steps are taken to create UWB operating frequency covering these frequencies.

In step 2, two square ring shaped slots are added in the middle which creates two parasitic patches in the radiating patch. The side of the square ring slots are calculated using the equation (4) [27], [28], [29].

$$S = \frac{c}{2f_s}\sqrt{\left(\frac{2}{1+\epsilon_r}\right)} \tag{4}$$

where S is the length of the side of the square ring slot and f_s is the resonance frequency. 7.7 *GHz* and 8.6 were chosen as the resonance frequencies for the single unit antenna square ring slots because these frequencies are adjacent to the higher order resonant frequencies achieved after step 1. The higher order resonance is used because at lower resonant frequencies the side of the square slots to achieve UWB results in a larger slot size which results in a larger back lobe [30]. The addition of the square ring slots reduces the side lobes and creates additional resonant frequencies [31], [32]. At the end of step 2 the single unit antenna achieves wideband resonances at 8.4 *GHz* and 9 *GHz* along with multiband resonances at 5.2 *GHz*, 5.7 *GHz*, 7.7 *GHz*, and 9.8 *GHz* as can be seen in Fig. 4(a). The SLL is also significantly reduced which can be observed from the radiation pattern in Fig. 4(b).

In step 3, two square ring slots are added on the top left and bottom right corners along with two *L*-shaped slots which are added at the top right and bottom left corners. The ring slot dimensions are similar to that of the 8.6 *GHz* ring slot resonator mentioned in step 2. The *L*-shaped slots added in the proposed antenna longer on one side so that the *L*-shape can cover a larger area in the rectangular radiating patch thus resulting in a higher current density in the center when coupled with the ring slots in the middle. The edges of slots added in the corner result in more current density compared to the antenna edges as can be seen in Fig. 3. The higher current density in the center of the antenna due to

the corner slots reduces the SLL and assists in creating a unidirectional radiation pattern [33]. The added corner slots also create a nonuniform current distribution direction within the antenna radiating patch which accommodates the increase in bandwidth [34], [35], [36]. A significant improvement in the S_{11} and radiation pattern can be observed after step 3. The single unit antenna achieves a UWB operating frequency of $7.7-8.7$ *GHz* along with multiband operations at 3.8 *GHz*, 5.2 *GHz*, 5.8 *GHz*, 6.3 *GHz*, and 9 *GHz* as depicted in Fig. 4(a). The radiation pattern also improves as the side lobes are reduced and a unidirectional radiation pattern can be observed after step 3 in Fig. 4(b). Although, the addition of the slots in step 3 increases the current density in the center of the antenna, the density value is higher near the feed compared to the top of the antenna as can be seen in Fig. 3. With the addition slots around the corners of the antenna and that the antenna feed is located slightly right from the center of the antenna, a higher current distribution can be observed on the left side of the antenna compared to the right side which can also be observed from Fig. 3. The higher current density near the feed coupled with the feed location being slightly towards the right compared to the center of the antenna results in a slightly tilted (by 12°) main lobe in the far-field radiation beam which can be observed in Fig. 4(b). In step 4 two rectangular slots are created in the ground plane placed at the top and at the bottom between the square and *L*-shaped corner slots. The addition of these slots creates an almost similar valued current distribution along the top and bottom of the radiating plane of the antenna. Another square slot is added in the ground plane at the center of the antenna which increases the current distribution at the center of the antenna. The slots added in the ground plane also increase the current density around the slots in the radiating patch as shown in Fig. 3. This reduces the SLL of the antenna and creates a more unidirectional radiation pattern. Although the current distribution after step 4 is improved and more symmetrical throughout the antenna, the antenna feed location still contributes to the tilting of the main radiating beam. The resultant far-field beam after step 4 is tilted by 6° which can be seen in Fig. 4(b). After the final design step as per simulation, the single unit antenna achieves a UWB operating frequency of $7.6-8.8$ *GHz*, a gain of 7.4 *dBi*, and a unidirectional radiation pattern as shown in Fig. 4(b). The performance comparison of the single unit antenna proposed in this paper with the state-of-the-art wideband antennas is provided in Table 1. Compared to the relevant wideband unit antennas, the proposed single unit antenna achieves an ultrawide bandwidth,high gain, and unidirectional radiation pattern. From Table 1 it can be observed that the ME dipole antenna presented in [22] achieves similar bandwidth performance within the UWB band. Although the electrical dimensions are similar, the physical dimension of the antenna is larger than the proposed single unit antenna where the λ is calculated for the center frequency. The proposed antenna also achieves 0.4 *dB* more gain than the antenna mentioned in [22] which results in 48% more gain when the 4×4 array is created. The proposed single unit antenna has a relatively simple structure and achieves such performance while maintaining the size restrictions for UAV placement.

TABLE 1. Performance comparison of the single unit antenna.

	Antenna Type	Dimension λ^2	Freq. (GHz)	Beam Dir	Gain (dBi)
[18]	Bow-tie	2.1×1.67	7.3-7.68	Bi	7
[19]	Bow-tie	0.5×0.3	5.2-5.8	Bi	4
[22]	ME Dipole	0.66×0.66	4.1-5.3	Uni	7
[23]	ME Dipole	1.1×1.1	1.58-2.79	Uni	7.8
[25]	U-slot	0.7×2.14	4.72-5.36	Omni	7.3
[24]	U-slot	1.2×0.86	9.4-10.5	Bi	6.6
This Work	**Modified Slot**	**0.73×0.58**	**7.6-8.8**	**Uni**	**7.4**

B. ANTENNA ARRAY DESIGN

The proposed 4×4 phased array antenna is designed using 16 single unit antennas detailed in the previous section placed with uniform spacing. In conventional narrowband phased array antennas, the array spacing is determined based on the single unit antennas' lower resonant frequency. In these cases, the single unit antennas are usually $< 0.5\lambda$ in size and are placed 0.5λ apart from center-to-center [37], [38]. The spacing between the single array element is kept $\leq \lambda$ to reduce the grating side lobes and achieve a lower SLL [39]. This approach is not suitable for UWB single unit antenna designed in this paper as the antenna size is $> 0.5\lambda$ for the antenna's UWB operating frequency and a higher array spacing results in a higher SLL. To overcome the aforementioned challenge, the array elements need to be increased which results in a larger antenna [40].

In order to achieve the optimum performance using the designed single unit antenna, this paper proposes an analysis to determine the array spacing based on the calculated gain of the 4×4 array which is further validated based on the gain, mutual coupling, and SLL of the 2×2 array. Based on the simulation based performance of the single unit antenna, the best UWB performance is achieved at a higher resonant band between $7.6 - 8.8$ *GHz*, where the antenna achieves a high gain and unidirectional radiation pattern. For this reason, to design the phased array antenna, 8 *GHz* is chosen as the center frequency of the UWB operating band. For 8 *GHz* operating frequency, the width and length of the single unit antenna can be represented as 0.74λ and 0.6λ, respectively. At first, the 4×4 phased array antenna gain, G_{PAA} is calculated using equations (5) and (6) [41], [42]:

$$G_{PAA} = |A.F.|^2 \times G_s \tag{5}$$

$$A.F. = \frac{sin\left(\frac{N}{2}(kd_e sin\theta cos\phi + \beta_x)\right)}{sin\left(\frac{1}{2}(kd_e sin\theta cos\phi + \beta_x)\right)} \tag{6}$$

where G_s is the gain of the single unit antenna and $A.F.$ is the array factor of the phased array antenna and it is dependent on the spacing between the single unit elements in

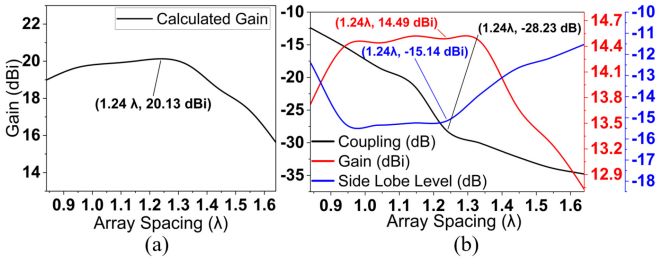

FIGURE 5. (a) Change in calculated gain of the 4 × 4 phased array with respect to spacing and (b) Simulated change in gain, coupling and side lobe level with respect to array spacing for a 2 × 2 quadrant.

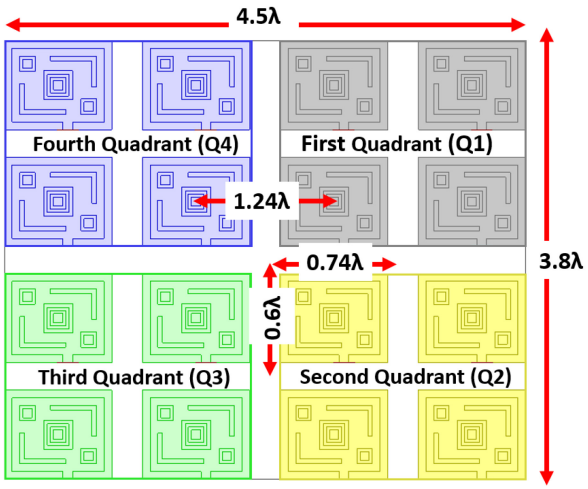

FIGURE 6. Proposed 4 × 4 phased array antenna.

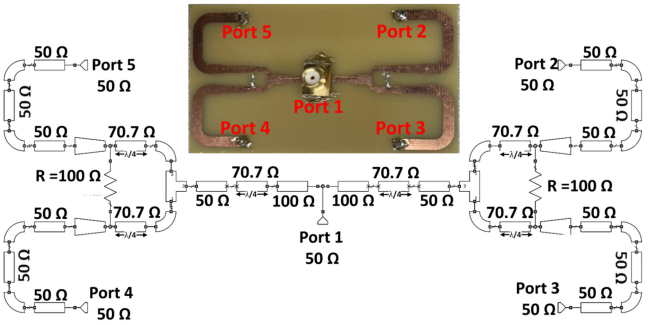

FIGURE 7. Circuit diagram and fabricated combiner for 2 × 2 array quadrant of the phased array antenna.

the antenna. The array factor, $A.F.$ is calculated using equation (6), where N is the number of single unit elements which is 16 in this design, k is the free space propagation constant, θ is the broadside beam direction along the elevation plane of the single element antenna, ϕ is the broadside beam direction along the azimuth plane of the single element antenna, β_x is the input phase difference between the single elements, and d_e is the distance between the single unit elements in a phased array. The calculated gain from equation (5) and (6) is shown in Fig. 5(a) for different spacing between the array elements when all the element has input phase difference equal to 0°. The calculation was done for $0.8\lambda - 1.6\lambda$ array spacing because with a lower array spacing, the designed single unit antennas will overlap. From 5(a) it is determined that at $d_e = 1.24\lambda$ spacing between the elements, the maximum gain is achieved. The calculated value was further verified using simulations. To validate the array element spacing, a 2 × 2 array quadrant of the 4 × 4 array is constructed and the gain, mutual coupling between the array elements and the SLL is observed by varying the array spacing between the elements. The spacing between the array elements is determined where the antenna achieves the maximum gain, low mutual coupling, and low SLL at the center frequency. The variance in gain, mutual coupling between array elements, and the SLL with respect to array element spacing are shown in Fig. 5(b). From Fig. 5(b) it can be observed that the 2 × 2 array achieves higher gain and low SLL for $0.97\lambda - 1.35\lambda$ and $0.94\lambda - 1.25\lambda$ respectively. Thus, for the 1.24λ array spacing the 2 × 2 array element achieves a high gain (14.49 dBi) with a low SLL (< -15 dB) and the mutual coupling is -28.23 dB, which is suitable for antenna array operation. Based on the analysis, the proposed 4×4 phased array antenna is created where the unit antennas are placed 1.24λ from center to center which results in 0.47λ spacing from edge to edge. The overall 4 × 4 array antenna is depicted in Fig. 6 where the total dimension of the antenna is $4.5\lambda \times 3.8\lambda$. The resultant dimension of the proposed 4 × 4 antenna is 17×14.3 cm^2 which falls within the size restrictions confined by small UAV's fuselage ($< 100 \times 40$ cm^2). The small size makes the proposed antenna suitable to be implemented in conventional small UAV.

C. COMBINER DESIGN

The 4 × 4 phased array antenna consists of 16 single unit antennas which have individual feeds. In order to provide signal feeding and achieve beam steering to the antennas in the 4 × 4 phased array, it is divided into four 2 × 2 array quadrants. Each 2 × 2 array is considered as a quadrant because if needed to be scaled up to provide wireless power to a larger UAV and/or provide wireless power at a longer distance, the scaling factor can be 2^n (where n = 1, 2, 3,. . .). This not only reduces the required number of active elements but also reduces the complexity for designing power dividers for feeding the antenna when being scaled up as the power dividers are also designed at 2^n rate. A 1 : 4 power divider is designed to feed the four antennas in each 2 × 2 array quadrant. The combiner is designed to provide equal power with no phase difference at each point and the dimensions of the microstrip lines were designed in a manner that the 4 ports of the combiner align perfectly with the 4 antennas in each 2×2 array quadrant. It consists of two Wilkinson power dividers which are connected by a 1 : 2 power divider. The circuit diagram and fabricated combiner circuit for the 2×2 phased array antenna along with the port numbers is depicted in Fig. 7. The combiner circuit is designed on FR4 substrate with 2 mm thickness and copper with 0.035 mm thickness is used as the radiating patch and the ground patch. The

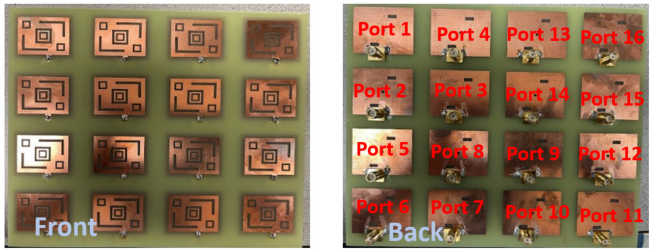

FIGURE 8. Fabricated 4 × 4 phased array antenna.

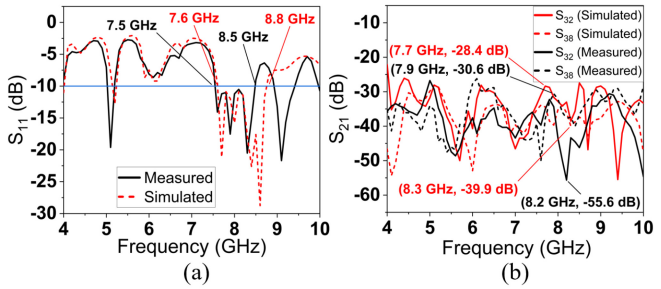

FIGURE 9. *S*-Parameters of the proposed 4 × 4 phased array antenna: (a) S_{11} of a single port and (b) mutual coupling between array elements.

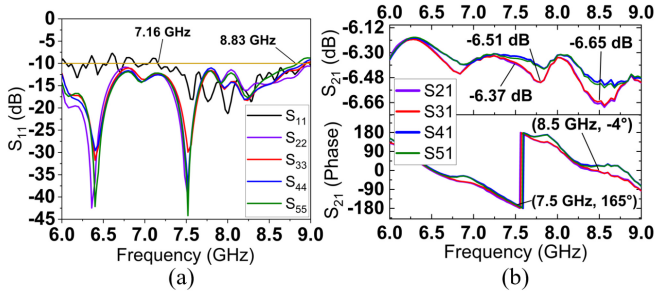

FIGURE 10. Measured *S*-Parameters of the 1 : 4 combiner: (a) S_{11} of each port, (b) S_{21} magnitude and phase between the input port and the output ports.

combiner circuit was designed on a thicker board because the transmission lines of the combiner are wider in 2 *mm* thick FR4 board which reduces the insertion loss of the combiner. All of the ports of the combiner is 50 Ω matched. The 1 : 4 combiner is custom designed to operate within the operating frequency of the proposed phased array antenna in order to reduce the loss due to the impedance mismatch between the combiner and the antenna that occurs while connecting the antenna with the combiners. At first, a Wilkinson 1 : 2 power divider was designed where the microstrip lines' widths were calculated considering 8 *GHz* as the center frequency. The 1 : 2 power divider worked at the center frequency and had a bandwidth of 1.7 *GHz*. The length of the output ports of the Wilkinson power divider was designed so that they align perfectly with the top and bottom antennas of the 2 × 2 sub-array as shown in Fig. 7. Afterwards the two designed Wilkinson power dividers were taken and fed with 100 Ω microstrip lines which are connected through quarter wavelength transformers to match with the 50 Ω input port of the combiner. The length of the 100 Ω microstrip lines were designed in such a way that all of the four output ports of the Wilkinson power divider align perfectly with the 2×2 quadrants. The 100 Ω lines are connected through a 50 Ω input port.

III. SIMULATION AND EXPERIMENTAL VALIDATIONS

The 4 × 4 phased array antenna proposed in this paper along with the combiners are fabricated according to the design parameters mentioned in Section II and the fabricated version of the antenna is depicted in Fig. 8. The design purpose of the antenna is to transmit wireless power over the UWB operating frequency range along with the electrical beam steering capability. The performance of the antenna is determined based on the return loss, gain, radiation pattern, and beam steering capabilities. The four quadrants of 2 × 2 array are named Q1, Q2, Q3, and Q4, respectively as depicted in Fig. 6. Each element within the quadrant is fed with the same input signal with the same phase. For the simulation in Ansys HFSS, the individual elements in the array were fed using lumped ports matched to 50 Ω. For the measurement, SMA connectors were used as the interface to feed the individual elements in the array. The SMA connectors which were used for the measurement was matched to 50 Ω as well.

A. S-PARAMETERS

The proposed antenna has 16 feeding ports for the 16 single elements of the 4 × 4 phased array. The return loss was measured for each port to determine the operating frequency of the antenna which remained almost constant for all the ports. The *S*-parameter measurements were performed using the ZVB40 4- port VNA from Rohde and Schwarz. The simulated and measured *S*-parameters of the proposed 4 × 4 phased array antenna are shown in Fig. 9. For the S_{11} analysis the frequency range < -10 *dB* has been considered as good matching because it yields to low return loss. Fig. 9(a) depicts the S_{11} of a single element antenna in the proposed phased array antenna and from there it can be observed that the proposed antenna achieves < -10 *dB* return loss over the UWB frequency range of $7.5 - 8.5$ *GHz*, which determines that the antenna achieves 1 *GHz* bandwidth with fractional bandwidth (FBW) of 12.5% within the UWB frequency band. Besides the UWB operating frequency, the antenna also achieves multiple resonating frequencies at 5.1 *GHz* (FBW = 2.4%) and 9.1 *GHz* (FBW = 6.6%). The $S_{3,2}$ and $S_{3,8}$, which represent the mutual coupling between the single elements of the proposed 4 × 4 phased array antenna, are shown in Fig. 9(b). It can be observed that the proposed phased array antenna achieves a measured port-to-port isolation $>$ 28.4 *dB* over the operating frequency band. The high port isolation reduces the mutual coupling coefficient between the adjacent single unit antennas in the phased array antenna.

The measured *S*-parameter performance of the combiner is depicted in Fig. 10. From Fig. 10(a) it can be observed

that the input port (Port 1) is perfectly matched and achieves < -10 dB return loss from $7.14 - 8.8$ *GHz*. The output ports connecting to the antenna have < -10 *dB* return loss over an UWB frequency range ($6 - 8.8$ *GHz*). Fig. 10(b) depicts the *S*-parameter magnitude and phase between the input port and output ports and the insertion loss of the combiner can be calculated from this figure as well. From Fig. 10(b) it can be observed that the combiner has insertion loss ranging from $0.33-0.65$ *dB* over the operating frequency of the proposed antenna. Fig. 10(b) shows that the output port of the combiner provides the same phased signal over the operating frequency.

B. GAIN AND RADIATION PATTERN

In order to measure the gain and the radiation pattern of the proposed antenna, all 16 ports are needed to be excited simultaneously. The designed combiner is used to feed all of the ports of the proposed 4×4 phased array antenna. Each of the four 2×2 array quadrants is connected with a combiner. At first, all of the single unit antennas in each quadrant are fed with the same input signal without any phase difference. The radiation pattern and gain for the proposed phased array antenna are measured for 0° phase difference in the input signals for all of the 16 ports of the proposed 4×4 phased array antenna. For this reason, the 4 combiners providing feed to 4 quadrants of the proposed phased array antenna are fed using another $1 : 4$ combiner. As a result, the input power from the source was divided into 16 equal portions, thus exciting the 16 feeds of the proposed phased array antenna with no input phase difference at each port. The radiation pattern and the gain are measured inside the anechoic chamber (RF Enclosures 18-5/5-0) by ETS Lindgren with microwave absorbers that enable the measurement of the radiation pattern from $D.C. - 40$ *GHz*. The gains and radiation patterns are measured using the DAMS 6050 automated antenna measurement system by Diamond Engineering which also calculates the radiation efficiency of the antenna. DAMS 6050 uses a standard antenna as the receiver while the antenna under test (AUT) rotates. In order to calculate the gain of the AUT, the gain values of the standard antenna needs to be uploaded into the controller software of DAMS 6050 as a dataset. The software calibrates the measurement based on the dataset to take into account the gain of the standard antenna similar to that of a two standard antenna approach for gain calculation. The proposed antenna is placed on the antenna measurement system and a standard horn antenna from RF Spin (Model: QRH40) is placed 1.3 *m* distance apart to measure the received signal. The proposed antenna has a calculated far-filed at > 1.1 *m* distance and the QRH40 horn antenna has a calculated far-field of > 0.1 *m*. Based on the far-fields of both antennas 1.3 *m* was chosen to accurately measure the radiation pattern and gain of the antennas. The DAMS antenna measurement system rotates the AUT instead of the reference antenna, making it hard to do the measurements of antennas with complex active circuits. As a result, the active circuits can not be covered by the absorbers and it results in a radiation pattern that is not smooth. The gain and radiation pattern measurement setup is shown in Fig. 11.

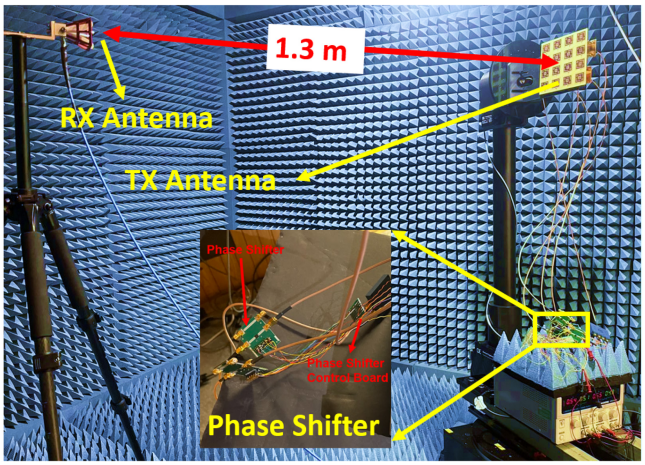

FIGURE 11. Radiation pattern measurement setup for the beam steering of the proposed 4 × 4 phased array antenna

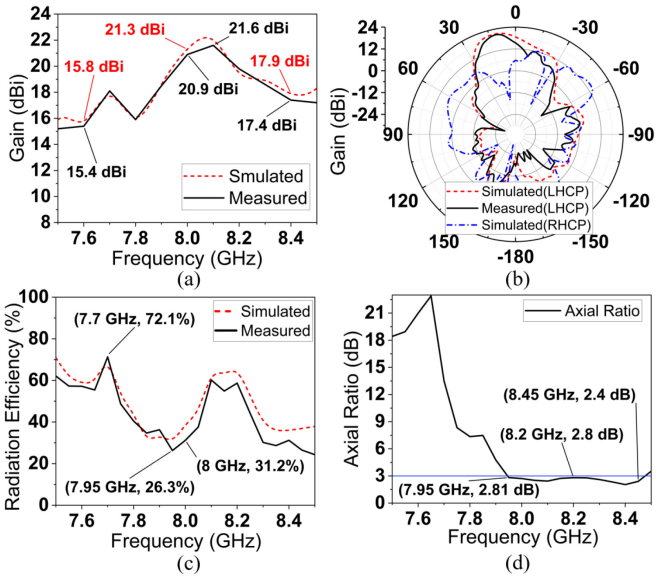

FIGURE 12. (a) Gain, (b) Radiation pattern along elevation plane at 8 *GHz* when the phase differences in all the ports are 0°, (c) Radiation efficiency, and (d) Axial ratio of the proposed 4 × 4 phased array antenna.

The simulated and measured gain of the proposed 4×4 phased array antenna over UWB operating frequency is depicted in Fig. 12(a). It can be observed that when the input signal phase has 0° degree phase difference between them, the highest gain of 21.6 *dBi* is achieved at 8.1 *GHz* frequency. From Fig. 12(a) it can also be observed that the gain of the proposed antenna ranged from $15.4 - 21.6$ *dBi* over the operating frequency band. The radiation pattern of the antenna at 8 *GHz* is depicted in Fig. 12(b), from which it can be determined that the antenna achieves a unidirectional radiation pattern with a half-power beamwidth (HPBW) of 28° and the broadside beam direction along

TABLE 2. Electrical beam steering achieved by the proposed antenna along θ-axis.

	7.6 GHz				8 GHz				8.4 GHz			
Input Phase Q1-Q2-Q3-Q4	Beam Dir. (θ)	HP-BW	Gain (dBi)	SLL (dB)	Beam Dir. (θ)	HP-BW	Gain (dBi)	SLL (dB)	Beam Dir. (θ)	HP-BW	Gain (dBi)	SLL (dB)
$90° - 90° - 0° - 180°$	$-27°$	28°	13	-10.2	$-24°$	26°	18.9	-14.7	$-18°$	22°	15.1	-13.4
$0° - 270° - 180° - 180°$	$-9°$	25°	14.9	-14.3	$-6°$	28°	19.6	-14.3	$-6°$	24°	16.2	-12.5
$0° - 0° - 0° - 0°$	9°	26°	15.4	-12.1	12°	25°	20.9	-19.7	11°	31°	17.4	-15.1
$180° - 10° - 270° - 180°$	21°	25°	14.2	-11.7	18°	24°	18.5	-12.3	24°	30°	16	-11.2
$90° - 0° - 180° - 0°$	33°	24°	13.2	-9.7	36°	32°	18.1	-12.4	36°	28°	14.6	-11.5

the 12° in the elevation plane. The radiation efficiency is shown in Fig. 12(c). The measured radiation efficiency was derived from the simulated directivity and the measured gain. From Fig. 12(c) it can be observed that the radiation efficiency of the antenna varies from $52.4\% - 77.5\%$ over the operating frequency. The highest radiation efficiency is achieved at 8.3 *GHz*. Fig. 12(d) depicts the simulated axial ratio of the proposed 4×4 phased array antenna. From the axial ratio, it can be concluded that the antenna is circularly polarized at $7.95 - 8.45$ *GHz*. As the feed of the single unit is located slightly right from the center of the antenna, it creates the nonuniform current distribution as shown in step 4 of Fig. 3. The location of the feed and the nonuniform current distribution results in left-hand circular polarization (LHCP) in the antenna. Fig. 12(b) also depicts the simulated LHCP and right-hand circular polarized (RHCP) radiation pattern of the antenna at 8 *GHz*, from which it can be observed that there is polarization isolation between LHCP and RHCP. The LHCP has higher gain and the radiation pattern is unidirectional. From this it can be presumed that the proposed antenna is left-hand circular polarized.

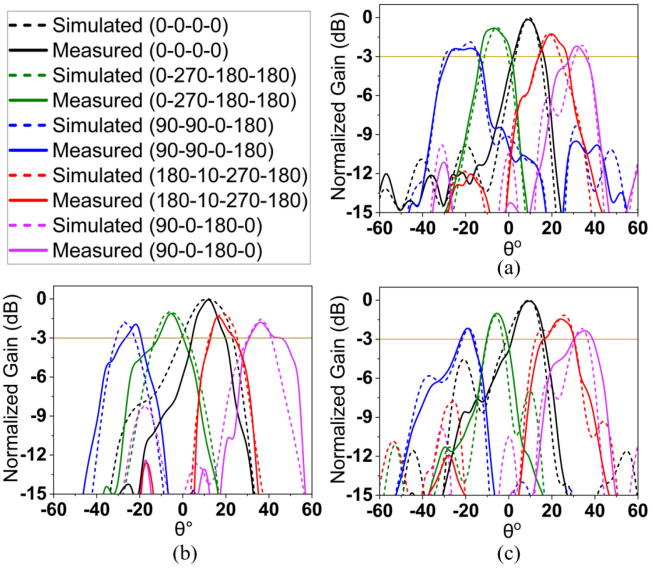

FIGURE 13. Simulated and Measured radiation beam steering of the proposed 4 × 4 phased array antenna along elevation plane (θ-axis) at (a) 7.6 *GHz*, (b) 8 *GHz*, and (c) 8.4 *GHz*.

C. BEAM STEERING

One of the main objectives of this work is to design an antenna with an electrical beam steering capability. The radiation beam of the proposed antenna can be electrically steered by providing phase difference at the input of each quadrant. An initial simulation based analysis was performed to realize the input phase difference combinations of the quadrants for which the antenna achieves almost similar beam scanning range along the elevation plane over the operating frequency band, which is experimentally validated afterward. Subsequently, another simulation based analysis is performed to determine the required phase difference combinations between the quadrants to steer the beam along the azimuth plane. Five phase difference value combinations between the four quadrants have been reported in this paper for azimuth and elevation steering to depict the total scanning range along with the scanning loss. In order to measure the beam steering characteristics of the proposed antenna, phase shifters are introduced to create phase differences between each quadrant input. To measure the beam steering of the antenna, four phase shifters are added at the input of each quadrant's combiner which is also shown in Fig. 11. The phase shifter used is MAPS-010146-001SMB from MACOM Technology Solutions and it is a $6 - bit$ phase shifter with 4.8 *dB* insertion loss and the capability of changing the phase of the input signal with 5.6° resolution. With the use of phase shifters, different phase combinations are provided at the four quadrants of the antenna, and the radiation pattern is measured along the azimuth and the elevation planes.

The electrical beam steering of the proposed antenna along the elevation plane at three different frequencies over the UWB frequency band (7.6, 8, and 8.4 *GHz*) and for different input phases at each quadrant is presented in Table 2. The simulated and measured beam steering along the elevation plane ($\theta - axis$) for the aforementioned frequencies is shown in Fig: 13. From Fig. 13 and Table 2 it can be observed that at the center frequency (8 *GHz*) the antenna has 20.9 *dBi* gain and a scanning range of 60° along the elevation plane. At 8 *GHz* the proposed antenna has a scanning loss of 2.4 *dB* and half power beam width (HPBW) ranging from $24° - 28°$. From Fig. 13 and Table 2 it can also be seen that at the lower (7.4 *GHz*) and higher (8.6 *GHz*) frequencies of the of the UWB operating band,

TABLE 3. Simulated beam steering along ϕ-axis for 8 *GHz*.

Input Phase Q1-Q2-Q3-Q4	Beam Dir.	HPBW ϕ	Gain (dBi)
$0^\circ - 180^\circ - 90^\circ - 270^\circ$	20°	42°	18.8
$0^\circ - 180^\circ - 0^\circ - 180^\circ$	0°	37°	19.3
$90^\circ - 270^\circ - 0^\circ - 180^\circ$	-20°	39°	19.9
$0^\circ - 270^\circ - 0^\circ - 60^\circ$	-45°	34°	20.3
$0^\circ - 0^\circ - 0^\circ - 0^\circ$	-75°	38°	20.9

the gain is decreased by 28.1% and 44.7%, respectively despite the scanning range remains above 54° along elevation plane. The scanning loss remains almost similar which is 2.3 *dB* and 2.8 *dB* at 7.4 *GHz* and 8.6 *GHz*, respectively and it can be concluded that the scanning loss of the proposed antenna increases with the frequency. The proposed antenna also achieves an SLL ranging from -9.7 *dB* to -19.7 *dB* over the operating frequency and the scanning range. The highest SLL is achieved at 7.6 *GHz* towards the 33° beam direction. Although the antenna achieved large SLL at 7.6 *GHz*, the scanning loss of the antenna is low which is more pivotal for far-field power beaming applications. From the above mentioned discussion, it can be concluded that the proposed planar 4×4 phased array antenna's radiation beam can be steered along the elevation plane over the UWB frequency ($7.4 - 8.5$ *GHz*) for the same quadrant input phase combinations. The proposed antenna achieves a scanning range from -24° *to* 36° along the elevation plane at the center frequency (8 *GHz*). The scanning range of the proposed antenna varies a little at the lower and upper frequencies within the band of the UWB operating frequency. Overall the proposed antenna achieves a consistent electrical scanning of -18° to 33° along the elevation plane throughout the frequency range of $7.6 - 8.4$ *GHz* band. The measurements were taken for five different phase combinations and these combinations were determined based on the simulation based analysis as mentioned before. For all these combinations, the proposed antenna covered the scanning range throughout the operating frequency.

To observe the beam steering along the azimuth plane (ϕ-axis) a simulation-based analysis is performed to determine the phase combinations at each quadrant. The required phase difference and far-field beam steering performance at 8 *GHz* of the proposed 4×4 phased array antenna is shown in Table 3 and Fig. 14. In the initial stage where there is no phase difference between the quadrants, the far-field beam is tilted along -75° along the azimuth plane. Based on the simulation-based analysis, with the phase combinations at each quadrant mentioned in Table 3 and Fig. 14, the antenna achieves an azimuth scanning range from -75° to 20°. The antenna achieves a wide HPBW ($> 34^\circ$) along the azimuth plane. When steered along the ϕ-axis, the antenna achieves a 2.1 *dB* scanning loss.

The group delay and phase delay of the proposed antenna is also characterized in this work. When implemented in an

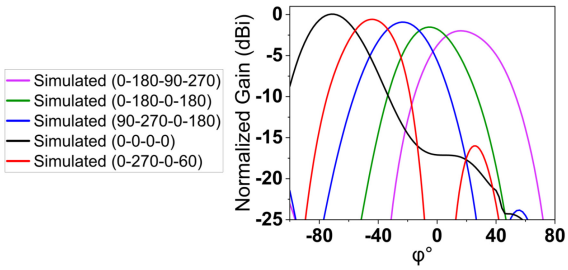

FIGURE 14. Simulated radiation beam steering of the proposed 4 × 4 phased array antenna along azimuth plane (ϕ-axis) at 8 *GHz*.

TABLE 4. Phase delay of the proposed antenna for the scan angles.

Input Phase	Phase Delay		
Q1-Q2-Q3-Q4	7.6 GHz	8 GHz	8.4 GHz
$0^\circ - 0^\circ - 0^\circ - 0^\circ$	246°	230°	93°
θ-axis Scanning			
$90^\circ - 90^\circ - 0^\circ - 180^\circ$	219°	230°	91°
$0^\circ - 270^\circ - 180^\circ - 180^\circ$	27°	58°	212°
$180^\circ - 10^\circ - 270^\circ - 180^\circ$	300°	317°	120°
$90^\circ - 0^\circ - 180^\circ - 0^\circ$	300°	29°	212°
ϕ-axis Scanning			
$0^\circ - 180^\circ - 90^\circ - 270^\circ$	82°	144°	332°
$0^\circ - 180^\circ - 0^\circ - 180^\circ$	192°	230°	90°
$90^\circ - 270^\circ - 0^\circ - 180^\circ$	165°	260°	90°
$0^\circ - 270^\circ - 0^\circ - 60^\circ$	192°	202°	120°

IR-UWB system, each quadrant of the antenna needs to be fed with a carrier-based impulse signal with the same time delay. A phase change is provided in the carrier signal to accommodate the beam steering. All of the quadrants of the antenna receive impulse signals at the same time with the same delay, same pulse width, and different carrier phases for different scanning angles. Due to the difference in the input carrier signal phase for different scanning angles, the resultant output signal from the antenna also has varying output signal phase, referred to as the phase delay. A transient simulation-based analysis has been conducted to calculate the group delay of the resultant transmitted signal of the proposed antenna for the different azimuth and elevation scanning angles. Table 4 represents the group delay or the output phase of the resultant transmitted signal for the different scanning range. The group delay of the proposed antenna is also calculated from the obtained phase delay values using the following equation (7) [43].

$$GroupDelay, T_g = \frac{1}{360^\circ} \times \frac{d\theta}{df} \tag{7}$$

where, $d\theta$ is the phase delay or the phase change in degrees and df is the delay in the frequency component in Hertz (Hz). The group delay for the proposed antenna at different scanning angle is listed in Table 5. Based on the simulated active *S*-parameter of the individual elements another analysis is performed to ascertain the effect on the input matching due to different input phase differences provided for the beam

TABLE 5. Group delay of the proposed antenna for the scan angles.

Input Phase	Group Delay (ns)		
Q1-Q2-Q3-Q4	7.6 GHz	8 GHz	8.4 GHz
$0° - 0° - 0° - 0°$	7.4	1.93	3.87
θ-axis Scanning			
$90° - 90° - 0° - 180°$	6.7	1.93	3.61
$0° - 270° - 180° - 180°$	0.82	0.52	8.83
$180° - 10° - 270° - 180°$	1.82	2.8	5
$90° - 0° - 180° - 0°$	1.82	0.24	8.83
ϕ-axis Scanning			
$0° - 180° - 90° - 270°$	2.46	1.2	13.8
$0° - 180° - 0° - 180°$	5.77	1.92	3.75
$90° - 270° - 0° - 180°$	4.96	2.16	3.75
$0° - 270° - 0° - 60°$	5.78	1.68	5

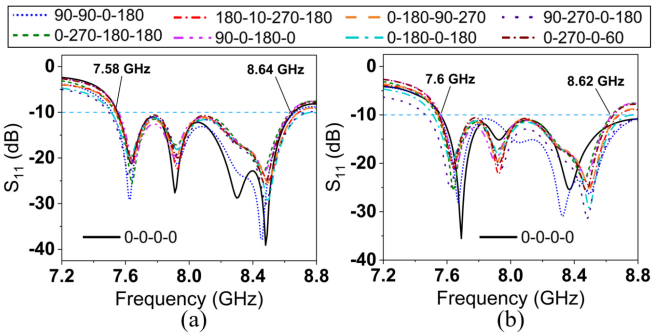

FIGURE 15. Simulated active *S*-parameter of (a) Port 1 and (b) Port 8 of the proposed 4 × 4 phased array antenna for different scan angles.

steering. The simulated active *S*-parameter of the proposed phased array antenna's port 1 and port 8 for different phase combinations is depicted in Fig. 15. Port 1 in the antenna represents the antenna array element located at the edge and port 8 in the antenna represents the antenna array element located in the center of the antenna surrounded by array elements with different input phases. From Fig. 15 it can be observed that the S_{11} for both ports remain within the performance range of the simulated S_{11} presented in Fig. 9(a) for the different phase combinations provided in order to induce beam steering.

D. WPT EXPERIMENT AND PATH LOSS MODELLING

Using the proposed 4×4 phased array antenna and a horn antenna a WPT system is developed. The ideal horn antenna used in this experiment is chosen to represent the receiving antenna of the UAV. The WPT system setup is similar to the radiation pattern measurement setup and the WPT measurements were performed for 1.3 m of distance as shown in Fig. 11 where the 4×4 phased array antenna and the QRH40 horn antenna have been used as the transmitter and receiver antennas respectively. The WPT system is measured for 0° phase difference at the input ports of the antenna. The WPT system's path loss is delineated based on the calculated and measured results for the UWB operating frequency band ($7.5 - 8.5$ GHz) and is based on the path loss

TABLE 6. Path loss characterization using proposed phased array antenna and QRG40 horn antenna.

	Calculated			Measured	
Freq (GHz)	RX Gain (dBi)	TX Gain (dBi)	Path Loss (dB)	Path Loss (dB)	PTE (%)
7.6	7.4	15.8	27.16	28.8	0.13
7.8	8.3	15.9	26.08	26.3	0.23
8	8.9	20.9	21.5	22.2	0.63
8.2	9.2	19.9	23.52	23.6	0.44

modeling in our previous work [49]. The WPT system losses include both path loss and combiner/splitter insertion loss. For this measurement, five combiners are required and all of their insertion losses combined were taken into account while performing path loss characterization. The phase shifters were removed for the WPT measurements as the beam steering was not required for this measurement. The path loss measurements are analyzed for the WPT system inside the anechoic chamber. Table 6 contains calculated WPT path loss with the combiner/splitter and measured path loss. The losses are measured for four different frequencies within the operating frequency band along with their calculated values. The free space path loss (FSPL) is calculated using the following equation:

$$FSPL = 20\log(d) + 20\log(f) + 20\log(4\pi/c) + G_t + G_r \tag{8}$$

where d is the distance between the antennas, f is the operating frequency, c is the speed of light and G_t, and G_r are the TX and RX antenna gains, respectively. The TX antenna gain is depicted in Fig. 12(a) and the RX gain values are taken from the datasheet of the QRH40 horn antenna by RF Spin. For the path loss characterization, a commercial horn antenna was used as the RX antenna which has a lower gain (< 8.5 dBi). The calculated and measured WPT system loss are almost similar and it can be observed in Table 6. The system loss and path loss of the WPT system vary from $22.2 - 28.8$ dB over $7.6 - 8.2$ GHz. Using the proposed antenna in a WPT system power transfer efficiency (PTE) of $0.13\% - 0.63\%$ can be achieved for the UWB operating range. The PTE is based on the path loss characterization with the assumption that 0 dBm power is being transmitted. The received power will increase if transmitted power is increased. When implemented in a distributed system with multiple transmitters power beaming a single receiver using IR-UWB signals, the PTE can be further improved by synchronizing the pulse and phases of the incident IR-UWB signals. In this paper commercial phase shifters are used to characterize the proposed antenna. The MAPS-010146-001SMB phase shifters are used for beam steering where each phase shifter has an insertion loss of 4.8 dB and it would add a total of 10.8 dB of loss in the system. So when the phase shifters are used, they will reduce the PTE by 12%. These phase shifters

TABLE 7. Comparison with state-of-the-art work.

	Technique	Dimension	Frequency (GHz)	FBW (%)	Gain (dBi)	Scanning Range	HP-BW	SLL (dB)	Rad. Eff.
[45]	Fluidically Programmable Metasurface on Planar Patch Antenna	$(120 \times 120 \times 6.8)\ mm^3$ $1.06\lambda \times 1.06\lambda \times 0.06\lambda$	2.58– 2.64	2.29	5.7	$-20°$ *to* $20°$	28°	–	–
[42]	Metasurface Lens Array on Phased Array Antenna	$(216 \times 72 \times 36)\ mm^3$ $7.2\lambda \times 2.4\lambda \times 1.2\lambda$	$9.1 - 11$	9.45	19.1	$-27°$ *to* $-3°$	16°	−10	65%
[46]	Interleaved Planar Subarray Antenna	$(216 \times 95 \times 0.79)\ mm^3$ $6.7\lambda \times 2.9\lambda \times 0.02\lambda$	$9 - 9.8$	8.51	20.6	$-14°$ *to* $14°$	8°	−19	36%
[47]	Phased Array Antenna with BST Thick Film Based Phase Shifter	$(70 \times 70 \times 2.16)\ mm^3$ $2.9\lambda \times 2.9\lambda \times 0.09\lambda$	$11.8 - 13$	9.67	11.1	$-25°$ *to* $25°$	18°	−14.1	–
[48]	Pind-diode Controlled Parasitic Layer on Planar Patch Antenna	$(60 \times 67 \times 10.81)\ mm^3$ $1\lambda \times 1.11\lambda \times 0.18\lambda$	$4.9 - 5.1$	4.16	8	$-40°$ *to* $40°$	40°	–	81%
[49]	Horn Antenna with Active Frequency Selective Surface	$(147 \times 147 \times 454)\ mm^3$ $2.64\lambda \times 2.64\lambda \times 8.2\lambda$	$5.2 - 5.6$	7.4	15.7	$0°$ *to* $31.5°$	48°	−19.8	44.6%
This Work	**Phased Array Antenna w 2×2 Array Quadrature Based Feeding and Phase Shift**	**(170×143×1.67) mm^3** **4.5λ×3.8λ×0.05λ**	**7.5−8.5**	**12.5**	**20.9**	**-24° to 36°**	**30°**	**-19.7**	77.5%

can be replaced by integrated IR-UWB transmitters with delay block-based phase shifters with low insertion loss and phase reconfigurability and high gain power amplifiers (PAs). An application specific on chip integrated transmitter along with the PA can reduce the insertion loss, provide precise phase for the beam steering, and make the system more compact thus increasing the efficiency of the overall system.

E. COMPARISON

The comparison of the proposed 4×4 phased array antenna with other state-of-the-art works implementing different method of beam steering is represented in Table 7. The proposed antenna achieves an UWB operating frequency with FBW $= 12.5\%$, which is $> 29\%$ higher than the UWB antennas proposed in [42] and [46]. The proposed antenna achieves a high gain of 20.9 *dBi*. Compared to the other state of the art works proposed in [42] and [45] the proposed phased array antenna achieves a higher gain ($> 1.5\%$) with $< 27\%$ smaller size. The proposed antenna also achieves up to 77.5% radiation efficiency which is higher than the mentioned state-of-the-art works. The proposed 4×4 phased array antenna also achieves a maximum 60° scanning range at 8 *GHz* and $> 51°$ scanning range over the UWB operating frequency with beamwidth ranging from $22° - 32°$ which is higher than the beam scanning array antennas reported in [44], [46], and [48]. The proposed antenna also achieves low SLL (-19.7 *dB*) at the center frequency with 0° phase difference between the elements which is higher than the other state-of-the-art works mentioned in Table 7.

IV. CONCLUSION

This paper proposes a 4×4 phased array antenna designed for far-field based impulse radio ultrawideband wireless power transfer applications. A step-by-step design analysis is provided for the single unit antenna where it is designed in such a way that it achieves a UWB operating frequency, unidirectional radiation beam, high gain, and a low SLL. As the single unit antenna dimension exceeds 0.5λ value for the center frequency of the UWB operation, an analysis is presented to figure out the optimized array spacing between the elements. The array spacing analysis is performed to achieve the highest gain and is based on calculation and validation from simulated results. The resultant antenna achieves an operating frequency of $7.5-8.5$ *GHz* with 12.5% FBW and a gain of 20.9 *dBi* at the center frequency. The antenna has been also designed to be used in the WPT application and the radiation beam of the proposed antenna can be steered. Each 2×2 subarray in the phased array is considered as a single quadrant. Four of these quadrants make up the whole 4×4 phased array. In order to steer the radiation beam in a certain direction, phase difference is created between the input signals at each quadrant. By controlling the input signal phase difference, the beam steering is also controlled to achieve a certain beam direction. A simulation based analysis was done to figure out the input phase combinations at each quadrant which would provide constant beam scanning over the operating frequency. The proposed phased array antenna has a beam scanning range of $> 51°$ along the elevation plane with an average beamwidth of 28° over the UWB operating frequency. The antenna also achieves $-75\ °$ to 20° scanning range throughout the azimuth plane at 8 *GHz*. The antenna has a radiation efficiency

ranging from $52.4\% - 77.5\%$ over the operating BW. With a smaller size, UWB operating frequency, higher gain, and constant beam scanning along the UWB operating frequency, the proposed phased array antenna is suitable for WPT applications. The antenna is designed with scalability in mind. Using the quadrant based feeding, the antenna can be further scaled up if required. The quadrant based beam steering reduces the active element requirements by $1/4^{th}$. A 0.63% WPT PTE has been achieved using the antenna and a commercial antenna. By implementing it at a larger scale the gain can be improved which will result in a higher PTE and the antenna can be implemented on larger UAVs.

REFERENCES

[1] T. W. R. East, "A self-steering array for the SHARP microwave-powered aircraft," *IEEE Trans. Antennas Propag.*, vol. 40, no. 12, pp. 1565–1567, Dec. 1992.

[2] N. Shinohara and S. Kawasaki, "Recent wireless power transmission technologies in japan for space solar power station/satellite," in *Proc. IEEE Radio Wireless Symp.*, 2009, pp. 13–15.

[3] A. P. Sample, B. H. Waters, S. T. Wisdom, and J. R. Smith, "Enabling seamless wireless power delivery in dynamic environments," *Proc. IEEE*, vol. 101, no. 6, pp. 1343–1358, Jun. 2013.

[4] J. Jadidian and D. Katabi, "Magnetic MIMO: How to charge your phone in your pocket," in *Proc. 20th Annu. Int. Conf. Mobile Comput. Netw.*, 2014, pp. 495–506. [Online]. Available: https://doi.org/10.1145/2639108.2639130

[5] N. Saha and I. Mahbub, "Design, modeling, and simulation of a 2.4 GHz near-field phased-array based wireless power transfer system for brain neuromodulation applications," in *Proc. IEEE Texas Symp. Wireless Microw. Circuits Syst. (WMCS)*, 2022, pp. 1–5.

[6] S. Y. Hui, "Planar wireless charging technology for portable electronic products and Qi," *Proc. IEEE*, vol. 101, no. 6, pp. 1290–1301, Jun. 2013.

[7] L. Liu, R. Zhang, and K.-C. Chua, "Multi-antenna wireless powered communication with energy beamforming," *IEEE Trans. Commun.*, vol. 62, no. 12, pp. 4349–4361, Dec. 2014.

[8] C.-J. Ahn, "Wireless power transmission with rough beamforming method," in *Proc. 2nd Nat. Found. Sci. Technol. Develop. Conf. Inf. Comput. Sci. (NICS)*, 2015, pp. 305–309.

[9] W. Liu, K. T. Chau, C. H. T. Lee, W. Han, X. Tian, and W. H. Lam, "Full-range soft-switching pulse frequency modulated wireless power transfer," *IEEE Trans. Power Electron.*, vol. 35, no. 6, pp. 6533–6547, Jun. 2020.

[10] A. B. Patwary, R. Mahin, and I. Mahbub, "A four channel impulse radio ultrawideband (IR-UWB) front end transmitter system for a 2×2 quadrature based phased array antenna designed in 180 nm CMOS process," in *Proc. IEEE Texas Symp. Wireless Microw. Circuits Syst. (WMCS)*, 2022, pp. 1–4.

[11] I. Güvenç and H. Arslan, "A review on multiple access interference cancellation and avoidance for IR-UWB," *Signal Process.*, vol. 87, no. 4, pp. 623–653, 2007.

[12] R. P. S. Ramesh and L. J. Muruga, "Mini unmanned aerial systems (UAV) - a review of the parameters for classification of a mini UAV," *Int. J. Aviation, Aeronaut., Aerosp.*, vol. 7, no. 3, p. 5, 2020.

[13] S. Nako, K. Okuda, K. Miyashiro, K. Komurasaki, and H. Koizumi, "Wireless power transfer to a microaerial vehicle with a microwave active phased array," *Int. J. Antennas Propagat.*, vol. 2014, pp. 1–5, Jan. 2014. [Online]. Available: https://www.hindawi.com/journals/ijap/2014/374543/

[14] A. B. Patwary, S. Abedin, and M. A. Hossain, "Design of a ladybug shaped circular polarized microstrip antenna at 5.8 GHz as microwave power transmitter to a MAV," in *Proc. Int. Conf. Elect., Comput. Commun. Eng. (ECCE)*, 2019, pp. 1–4.

[15] D. Belo, D. C. Ribeiro, P. Pinho, and N. B. Carvalho, "A selective, tracking, and power adaptive far-field wireless power transfer system," *IEEE Trans. Microw. Theory Tech.*, vol. 67, no. 9, pp. 3856–3866, Sep. 2019.

[16] B. Yang, X. Chen, J. Chu, T. Mitani, and N. Shinohara, "A 5.8-GHz phased array system using power-variable phase-controlled magnetrons for wireless power transfer," *IEEE Trans. Microw. Theory Tech.*, vol. 68, no. 11, pp. 4951–4959, Nov. 2020.

[17] A. B. Patwary and I. Mahbub, "Design and simulation of UWB phased array antenna for wireless power transfer to micro aerial vehicle (MAV) through beam steering," in *Proc. IEEE Radio Wireless Symp. (RWS)*, 2022, pp. 111–114.

[18] D. Li and J.-F. Mao, "A koch-like sided fractal bow-tie dipole antenna," *IEEE Trans. Antennas Propag.*, vol. 60, no. 5, pp. 2242–2251, May 2012.

[19] M.-T. Wu and M.-L. Chuang, "Multibroadband slotted bow-tie monopole antenna," *IEEE Antennas Wireless Propag. Lett.*, vol. 14, pp. 887–890, 2015.

[20] Y.-Y. Jeong and W.-S. Lee, "Wideband printed half bow-tie antenna array based on a quad-mode reconfigurable feeding network for UAV communications," *IEEE Open J. Antennas Propagat.*, vol. 2, pp. 238–248, 2021.

[21] S. Song, X. Chen, Y. Da, and A. A. Kishk, "Broadband dielectric resonator antenna array with enhancement of isolation and front-to-back ratio for MIMO application," *IEEE Antennas Wireless Propag. Lett.*, vol. 21, pp. 1487–1491, 2022.

[22] C. Song, E. L. Bennett, J. Xiao, and Y. Huang, "Multimode hybrid antennas using liquid dielectric resonator and magneto-electric dipole," *IEEE Trans. Antennas Propag.*, vol. 69, no. 6, pp. 3132–3143, Jun. 2021.

[23] G. Zhang, L. Ge, J. Wang, and J. Yang, "Design of a 3-D integrated Wideband filtering magneto-electric dipole antenna," *IEEE Access*, vol. 7, pp. 4735–4740, 2019.

[24] M. Teng, S. Yu, N. Kou, Z. Ding, and Z. Zhang, "Mechanical beam steering array antenna with tunable height," *IEEE Antennas Wireless Propag. Lett.*, vol. 21, pp. 2293–2297, 2022.

[25] S. Liu, S.-S. Qi, W. Wu, and D.-G. Fang, "Single-feed dual-band single/dual-beam U-slot antenna for wireless communication application," *IEEE Trans. Antennas Propag.*, vol. 63, no. 8, pp. 3759–3764, Aug. 2015.

[26] B. Zhang and X. Xu, "Low profile broadband phased array antenna designed with U-slot patch antennas," in *Proc. Cross Strait Radio Sci. Wireless Technol. Conf. (CSRSWTC)*, 2020, pp. 1–3.

[27] C. A. Balania, *Antenna Theory: Analysis and Design*. Hoboken, NJ, USA: Wiley, 2016.

[28] A. B. Patwary and I. Mahbub, "Design, simulation and comparison of two 15mm × 15mm UWB antennas with modified ground patch for high data-rate wireless electrophysiological recording application," in *Proc. IEEE Texas Symp. Wireless Microw. Circuits Syst. (WMCS)*, 2021, pp. 1–6.

[29] K. Kandasamy, B. Majumder, J. Mukherjee, and K. P. Ray, "Dual-band circularly polarized split ring resonators loaded square slot antenna," *IEEE Trans. Antennas Propag.*, vol. 64, no. 8, pp. 3640–3645, Aug.2016.

[30] W.-J. Lui, C.-H. Cheng, and H.-B. Zhu, "Improved frequency notched ultrawideband slot antenna using square ring resonator," *IEEE Trans. Antennas Propag.*, vol. 55, no. 9, pp. 2445–2450, Sep. 2007.

[31] H.-T. Chou, "Radiation sidelobe reduction and focus properties of reflector antennas by grating the aperture field via nonperiodic fresnel-zone plate lens," *IEEE Trans. Antennas Propag.*, vol. 66, no. 5, pp. 2634–2639, May 2018.

[32] Y. Kimura, K. Furukawa, S. Saito, Y. Kimura, and T. Fukunaga, "Design of wideband multi-ring microstrip antennas fed by an L-probe for single-band and dual-band operations," in *Proc. IEEE Int. Symp. Antennas Propagat. North Amer. Radio Sci. Meet.*, 2020, pp. 541–542.

[33] S. K. Sharma, L. Shafai, and N. Jacob, "Investigation of wide-band microstrip slot antenna," *IEEE Trans. Antennas Propag.*, vol. 52, no. 3, pp. 865–872, Mar. 2004.

[34] R. Ferreira, J. Joubert, and J. W. Odendaal, "A compact dual-circularly polarized cavity-backed ring-slot antenna," *IEEE Trans. Antennas Propag.*, vol. 65, no. 1, pp. 364–368, Jan. 2017.

[35] Y. J. Sung, "Bandwidth enhancement of a wide slot using fractal-shaped Sierpinski," *IEEE Trans. Antennas Propag.*, vol. 59, no. 8, pp. 3076–3079, Aug. 2011.

[36] S. Sadat, M. Fardis, F. Geran, G. Dadashzadeh, N. Hojjat, and M. Roshandel, "A compact microstrip square-ring slot antenna for UWB applications," in *Proc. IEEE Antennas Propagat. Soc. Int. Symp.*, 2006, pp. 4629–4632.

[37] A. Ludvig-Osipov, J.-M. Hannula, P. Naccachian, and B. L. G. Jonsson, "Physical limitations of phased array antennas," *IEEE Trans. Antennas Propag.*, vol. 69, no. 9, pp. 5512–5523, Sep. 2021.
[38] R. Çetiner, A. Hizal, and R. F. Tiğrek, "Narrow band wide angle scanning circular frequency diverse array radar," in *Proc. Eur. Radar Conf. (EURAD)*, 2017, pp. 231–234.
[39] R. Munson, "Microstrip phased array antennas," in *Proc. EIC 11th Elect. Insul. Conf.*, 1973, pp. 281–283.
[40] H. Holter and H. Steyskal, "On the size requirement for finite phased-array models," *IEEE Trans. Antennas Propag.*, vol. 50, no. 6, pp. 836–840, Jun. 2002.
[41] R. J. Mailloux, *Phased Array Antenna Handbook*. Norwood, MA, USA: Artech House, 2017.
[42] R. Xu and Z. N. Chen, "A compact beamsteering metasurface lens array antenna with low-cost phased array," *IEEE Trans. Antennas Propag.*, vol. 69, no. 4, pp. 1992–2002, Apr. 2021.
[43] Keysight. "Group delay." Accessed: Dec. 10, 2023. [Online]. Available: https://rfmw.em.keysight.com
[44] A. H. Naqvi and S. Lim, "A beam-steering antenna with a fluidically programmable metasurface," *IEEE Trans. Antennas Propag.*, vol. 67, no. 6, pp. 3704–3711, Jun. 2019.
[45] A. Abbaspour-Tamijani and K. Sarabandi, "An affordable millimeter-wave beam-steerable antenna using interleaved planar subarrays," *IEEE Trans. Antennas Propag.*, vol. 51, no. 9, pp. 2193–2202, Sep. 2003.
[46] M. Nikfalazar et al., "Two-dimensional beam-steering phased-array antenna with compact tunable phase shifter based on BST thick films," *IEEE Antennas Wireless Propag. Lett.*, vol. 16, pp. 585–588, 2017.
[47] M. A. Towfiq, I. Bahceci, S. Blanch, J. Romeu, L. Jofre, and B. A. Cetiner, "A reconfigurable antenna with beam steering and beamwidth variability for wireless communications," *IEEE Trans. Antennas Propag.*, vol. 66, no. 10, pp. 5052–5063, Oct. 2018.
[48] W. Pan, C. Huang, P. Chen, M. Pu, X. Ma, and X. Luo, "A beam steering horn antenna using active frequency selective surface," *IEEE Trans. Antennas Propag.*, vol. 61, no. 12, pp. 6218–6223, Dec. 2013.
[49] B. A. Patwary, R. Mahin, and I. Mahbub, "Path loss Characterization for a pulse-based wireless power transfer system using ultrawideband (UWB) phased array antenna," in *Proc. IEEE Int. Symp. Antennas Propagat. USNC-URSI Radio Sci. Meet. (AP-S/URSI)*, 2022, pp. 1–2.

ADNAN BASIR PATWARY (Member, IEEE) received the B.Sc. degree in electronics and telecommunication engineering from the Chittagong University of Engineering and Technology, Chittagong, Bangladesh, in 2017. He is currently pursuing the Ph.D. degree in electrical engineering with the Department of Electrical and Computer Engineering, The University of Texas at Dallas, Richardson, TX, USA, where he is also a Graduate Research Assistant with Integrated Biomedical RF Circuits and Systems Laboratory. His research focuses on antenna design, electro-mechanical beamforming, waveform engineering, and CMOS RF transmitter circuit development for far-field ultrawideband communication and wireless power beaming. He is the recipient of the 2022 Student Travel Grant presented by the IEEE Antennas and Propagation Society. He was awarded the First Prize for 2022 Outstanding Graduate Research by the College of Engineering at the University of North Texas and placed in the top 15 of The University of Texas at Dallas Research Day poster competition.

IFANA MAHBUB (Senior Member, IEEE) received the B.Sc. degree in electrical and electronic engineering from the Bangladesh University of Engineering and Technology in 2012, and the Ph.D. degree in electrical engineering from the University of Tennessee, Knoxville, in 2017. She is an Assistant Professor and the Texas Instrument's Early Career Chair Awardee with the Department of Electrical and Computer Engineering, The University of Texas at Dallas, where she is leading the Integrated Biomedical, RF Circuits and Systems Laboratory. She has published two book chapters, 29 journal publications, and over 62 peer-reviewed conference publications. Her research interests include energy-efficient integrated circuits and systems design for read-out, wireless communication, and wireless power transfer for various implantable and wearable sensors. Her recent research interests also include ultrawideband/mm-wave phased-array antenna design for far-field wireless power transfer/V2V communication for UAVs. She is the recipient of the NSF "Early Career Award" in 2020, and the DARPA "Young Faculty Award" in 2021. She has served as the Publicity Chair for the IEEE Dallas Circuits and Systems Society. She also serves as the Secretary for the URSI Commission K, as a Guest Editor for the IEEE OPEN JOURNAL OF ANTENNAS AND PROPAGATION and *Sensors* (MDPI), as a Young Professional Co-Chair for the IEEE Sensors Conference, and as the Publications Chair for the IEEE Texas Symposium on Wireless and Microwave Circuits and System and IEEE Dallas Circuits and System Conferences.